Corrosion Sensor Using Metallic Double Layer in Optical Fiber

Hebio J. B. de Oliveira[1] ⓘ, Elias A. Silva-Jr[1] ⓘ, Henrique P. Alves[1] ⓘ, Jehan F. do Nascimento[2] ⓘ,
Luis H. Vilela-Leão[2] ⓘ, Charlie S. Gonçalves[3] ⓘ, Joaquim F. Martins-Filho[1] ⓘ

[1]Department of Electronics and Systems, Federal University of Pernambuco. Recife, Brazil
hebio.junior@ufpe.br, arcanjoelias@hotmail.com, henrique.patriota@ufpe.br, joaquim.martins@ufpe.br
[2]Interdisciplinary Nucleus for Exact and Natural Sciences, Federal University of Pernambuco. Caruaru, Brazil
jehan.nascimento@ufpe.br, luis.leao@ufpe.br
[3]Departament of Physics, Federal University of Paraiba. João Pessoa, Brazil,
charlie@fisica.ufpb.br

Abstract— **In this paper, a new optical fiber corrosion sensor based on metallic bilayers is described. The detection region is located at a fiber end facet and we present simulations as well as experimental results in controlled lab conditions for Ti(10 nm)/Al(10 nm) and Ni(5 nm)/Al(5 nm) bilayers. We perform the characterization of the device by numerical simulations using the COMSOL Multiphysics software, and with an analytical model, which makes use of the Fresnel equations. According to the simulations, the change in the reflected optical signal over time is related to variations in the thickness of the metallic films by the corrosive process and, consequently, the corrosion rate in each metal of the bilayer can be obtained. Upon the simulation results, sensor devices were fabricated by depositing thin metallic films on the cleaved facet of the optical fiber using the sputtering method. We show that the use of a metallic bilayer as a transducer, instead of a monolayer, improves the sensor measuring interval (20 ± 1 nm) and provides information about the corrosion rate along the corrosion process.**

Index Terms—corrosion, double layer, optical fiber, sensor.

I. INTRODUCTION

Corrosion is one of the main degradation mechanisms that affect industrial structures, whether they are static, such as bridges, gas pipes, oil pipelines, that normally operate in a highly corrosive environment, as well as mobile transport structures, such as ships or aircrafts [1]. The knowledge of the evolution of the corrosive process allows one to minimize the risk of failures caused in the structure and, therefore, reduces the need to carry out unscheduled interventions, allowing a proactive maintenance of the structures, with gains related to the level of control and scheduling of operations. Therefore, the monitoring of localized corrosion problems in a structure can contribute to making maintenance more efficient, allowing the maintenance effort to be concentrated in the neediest areas [2].

There are many techniques for corrosion monitoring, some have been widely used, such as linear polarization resistance, polarization curves, electrochemical impedance spectroscopy, among others

[3], [4]. However, sensing techniques based on optical fibers have advantages such as simplicity, versatility, safety, reliability, distributed measurement, immunity to external electromagnetic interference and ability to resist hostile environments. For this reason, some optical fiber sensors are commercially available [5], [6]. In addition, the use of fiber optics allows signals to be transmitted over long distances with low loss, enabling a remote monitoring system. As such, it is suitable for use in highly controlled environments such as nuclear or chemical plants [7]. Currently, optical fiber-based sensors are used to monitor various physical and chemical properties such as humidity [8], microbends [9], [10], electric field [11], [12], temperature [13], [14], pressure [15], magnetic field [16], gas [17], [18], corrosion [19]-[21] among others.

In recent years, corrosion monitoring systems using optical fiber have attracted attention [22]. There are reports in the literature of the use of optical fibers with metallized cleaved facet to create the sensor region [19], [23], [24]. These sensors use the optical time domain reflectometry (OTDR) technique as the interrogation method, which provides multi-point monitoring. The results presented in these types of systems showed the possibility of obtaining the corrosion rate of the metallic thin film from kilometers distance of the monitoring point [19]. However, in these systems, there is an operational limitation that consists of a monitoring period without detecting the onset of corrosion. This occurs because, at the beginning of the corrosion process, the metallic film on the cleaved fiber is still too thick to generate changes in the amplitude of the reflected optical signal in the sensor element [19].

In this paper, we propose a corrosion sensor using an optimized metallic bilayer on the cleaved facet of a single-mode optical fiber. We present simulations as well as experimental results in controlled lab conditions for Ti(10 nm)/Al(10 nm) and Ni(5 nm)/Al(5 nm) bilayers. The thickness and composition of the metallic layers were optimized via simulations. The sputtering deposition process was used for the fabrication of the metallic bilayer on the fiber facet. The performance characteristics of the sensor are shown experimentally in accelerated corrosion tests in the laboratory. The use of a bilayer, instead of a monolayer as in previous publications, improves the sensor measuring interval, mitigating the sensor blind period problem identified in monolayer structures, and provides the corrosion rate earlier during the corrosion process.

II. Device Modeling

A. Analytical Model

The longitudinal section of an optical fiber with a metallic bilayer over one of its extremities is illustrated in Fig. 1 (a), which represents the sensor element of the corrosion detection system described in this work. In this structure, the optical signal guided in the optical fiber is affected by the metallic bilayer, causing a fraction of that signal to be reflected, another fraction is absorbed and, depending on the thickness of the bilayer, a fraction of the signal is transmitted to the external media. Under the action of a corrosive process, the reduction of the thickness of the metals that make up the

bilayer causes a modulation in the intensity of the reflected optical signal. This modulation can be obtained, theoretically, based on the Fresnel equations for reflection [23], [25], by approximating the sensor element of Fig. 1 (a) by a multilayer system, as illustrated in Fig.1 (b). As can be seen in Fig. 1 (b), the multilayer system is composed of silica (fiber core material), metal 1, metal 2 and external medium (corrosive agent).
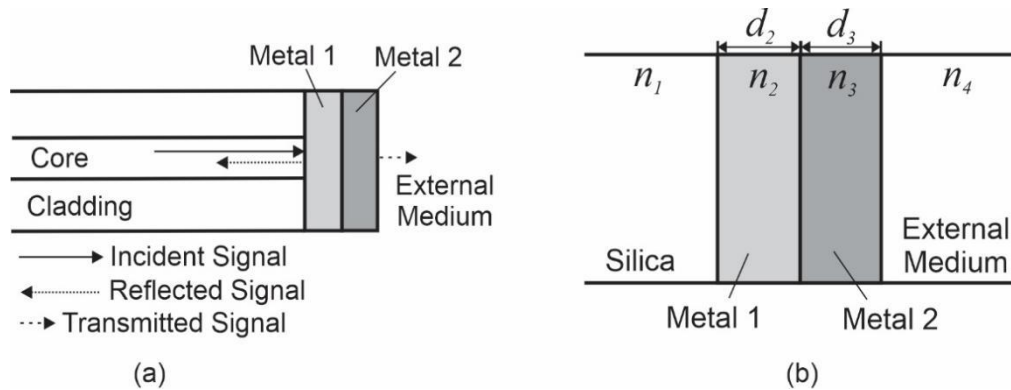

Fig. 1. (a) Sensor element with metallic bilayer. (b) Multilayer system used by the analytical model.

The modulation of the reflected optical signal can be analyzed through the reflectance, R, for the multilayer system [23], [25], defined as

$$R = \left| \frac{r_{12} + r_{23}e^{-j\Phi_2} + r_{34}e^{-j(\Phi_2+\Phi_3)} + r_{12}r_{23}r_{34}e^{-j\Phi_3}}{1 + r_{12}r_{23}e^{-j\Phi_2} + r_{12}r_{34}e^{-j(\Phi_2+\Phi_3)} + r_{23}r_{34}e^{-j\Phi_3}} \right|^2, \tag{1}$$

where r_{12}, r_{23} and r_{34} are the reflection coefficient in the simple interfaces, silica/metal 1, metal 1/metal 2 and metal 2/external medium, respectively, defined in a generic way for normal incidence, as

$$r_{ij} = \frac{n_i - n_j}{n_i + n_j}, \tag{2}$$

with $(i,j)=\{(1,2); (2,3); (3,4)\}$. The phase change for the electromagnetic wave that penetrates metals 1 and 2 is given by Φ_2 and Φ_3 [23], [25], respectively, defined as

$$\Phi_k = \frac{4\pi n_k d_k}{\lambda}, \tag{3}$$

where n_k and d_k are the refractive index and thickness of the k-th metallic medium of the multilayer system, respectively, with $k=\{2,3\}$, and λ is the wavelength of the optical signal. From the expressions (2) and (3), the reflectance R in (1) is explicitly defined. It can be seen in (1) that, as the thickness of thin metal films is reduced, it is possible to analyze the variation of reflectance R. Consequently, the corrosion process in thin metal films can be detected by changes in the intensity of the reflected optical signal.

B. Numerical Model

In this section, a modeling for the corrosion dynamics of the transducer elements of the corrosion sensor is presented, considering the generation of the roughness on the surface of these transducers due to the corrosive process. In general, surface roughness can be considered as a non-Euclidean

irregular geometry [26]. Its structure may show randomness or similarity and, in this sense, the surface roughness can be treated as a fractal type geometry [26]. These geometric shapes are seen in many chemical and physical phenomena, such as thin film growth, erosion [27] and corrosion [28]. In the literature, two classic fractal functions are found that can represent the surface roughness: Weierstrass fractal and Weierstrass-Mandelbrot fractal [26]. These functions are represented by infinite series of sinusoidal functions, which model the surface roughness by a complex periodic structure [26]. However, some works obtained in the literature make a simpler approach to surface roughness, through a sinusoidal function [29]. This function, called the roughness function, R (d, s), is defined in (4), and models the dynamics of the corrosion process of the metal transducers of the optical sensor based on the creation of peaks and valleys on the surface of these transducers, as illustrated in Fig. 2.

$$R(d,s) = A(d)\sin\left(\frac{2\pi}{\Lambda} n_{ext} s\right) + d , \qquad (4)$$

where d is the average thickness of the metallic films, which decreases over the corrosive process; $A(d)$ is the roughness amplitude, which is a function of d; Λ is the periodicity of the rough surface; s is a scanning parameter in the range [0,D_{clad}], where D_{clad} is the diameter of the optical fiber. The parameter n_{ext} is interpreted as a scale factor and assumes the value of the refractive index of the external medium, as used in [29]. Some parameters of the roughness function are highlighted in Fig. 2.
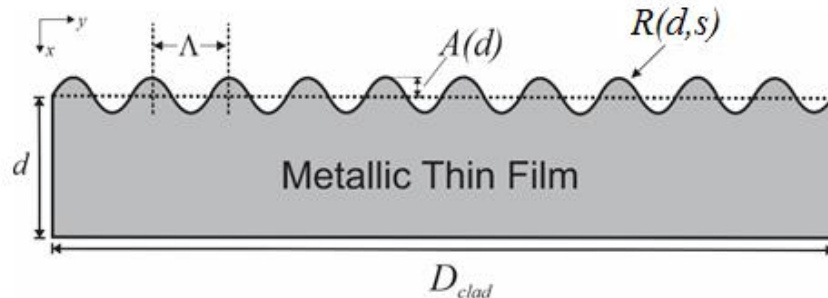

Fig. 2. Proposed morphology for surface roughness generated in metallic films [26].

From the methodology proposed in [29], the values for $A(d)$ and Λ, of the function $R(d,s)$, are defined by comparing the values of the intensity of the reflected optical signal obtained by the computational model with the measured values experimentally, throughout the corrosion process. In other words, values for these parameters are assigned in such a way that the computational result approaches the experimental result [29].

The numerical modeling for the sensor element of the corrosion detection system, proposed in this work, was implemented in COMSOL Multiphysics, which is a software based on the finite element method (FEM). To study the propagation of electromagnetic waves with optical frequencies in waveguides the Wave Optics module [30] was used. The 2D geometry of the implemented model is shown in Fig. 3, which represents the longitudinal section of a single-mode optical fiber with a

metallic bilayer on its cleaved facet (right end). The layer of the core, the shell, the external environment (corrosive agent) and the metallic films, which define the structure of the model, are highlighted in Fig. 3. By zooming in on the transducer region, one can see the rough surface of the metal films, modeled by the roughness function (4). In the simulation, two types of metallic bilayers are used: titanium/aluminum (Ti/Al) and nickel/aluminum (Ni/Al).
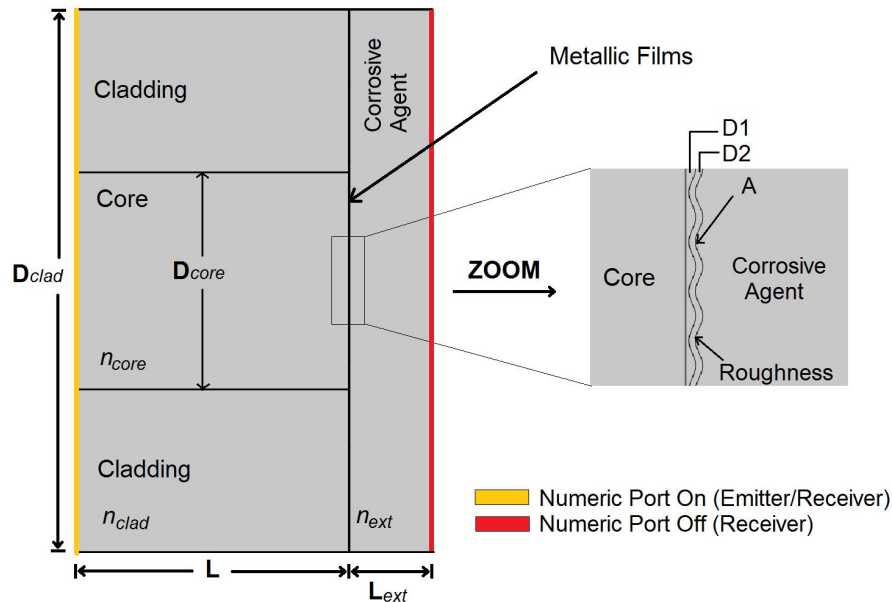

Fig. 3. Diagram of 2D computational modeling of the sensor element with double metallic layer.

Defining the left end of the 2D structure shown in Fig. 3 as a Numerical Port [30] in COMSOL, configured as an emitter, a non-polarized optical signal with a wavelength of 1550 nm is emitted from that end, establishing the fundamental propagation mode at the core of the optical fiber structure. The measurement for the reflected optical signal is also performed by the left end Numerical Port, configured as a detector. This measure is obtained from the scattering parameter S_{11} [30]. This parameter corresponds to the reflection coefficient [30], so that the reflectance R is given by $R=||S_{11}||^2$.

Table I provides the values for the optical and geometric parameters used in computational modeling. For the fiber cladding layer, with width D_{clad}, the reduced value of 20 μm was used to limit the use of RAM memory to solve the numerical model. There is not loss of generality with this approximation, as the light penetration length in the cladding for the wavelength of 1550 nm is lower than this value [31]. The wavelength of light at 1550 nm was chosen because it is the one with the lower propagation loss in optical fiber and the one with the greatest availability of optical fiber emitting, receiving and coupling devices, facilitating the construction of sensor systems. For the discretization of the 2D geometry of Fig. 3, for the use of the FEM, a triangular mesh with finite element size given by $\lambda/200$ was used for the layers of thin metallic films. For the fiber core, cladding and the external environment, a triangular mesh with a size of $\lambda/30$, was used, where λ is the

wavelength of the optical signal. These finite element sizes are in accordance with the conditions suggested in [30] to solve the problem of propagation of electromagnetic waves with optical frequencies in waveguides.

TABLE I. OPTICAL AND GEOMETRIC PARAMETERS [32]-[36]

Description	Parameter	Value
Wavelength	λ	1550 nm
Refractive index of the core, at 1550 nm	n_{core}	1.4443
Refractive index of the cladding, at 1550 nm	n_{clad}	1.4378
Aluminum refractive index, at 1550 nm	n_{Al}	$1.3474 - j14.133$
Titanium refractive index, at 1550 nm	n_{Ti}	$3.4323 - j3.1162$
Nickel refractive index, at 1550 nm	n_{Ni}	$3.4418 - j6.7542$
Core diameter	D_{core}	8 μm
Cladding diameter	D_{clad}	20 μm
Optical fiber length	L	10 μm
External medium length	L_{ext}	3 μm
Refractive index of the Al-etch	n_{ext}	1.38
Refractive index of the Si Iso etch	n_{ext}	1.376
Metal 1 thickness	$D1$	-
Metal 2 thickness	$D2$	-

III. EXPERIMENTAL SETUP

The experimental setup used in this work to characterize the sensors consists of a diode laser connected to the sensor under test and an optical spectrum analyzer (OSA) through an optical circulator, as illustrate in Fig. 4. The optical circulator directs the laser light to the sensor region and directs the light reflected by the sensor region to the OSA. The OSA data is sent to a computer for processing and determination of the corrosion rate. The laser operates at a wavelength of 1550 nm with a power of 10 mW. The circulator and optical fiber are standard devices used in the telecommunication industry.
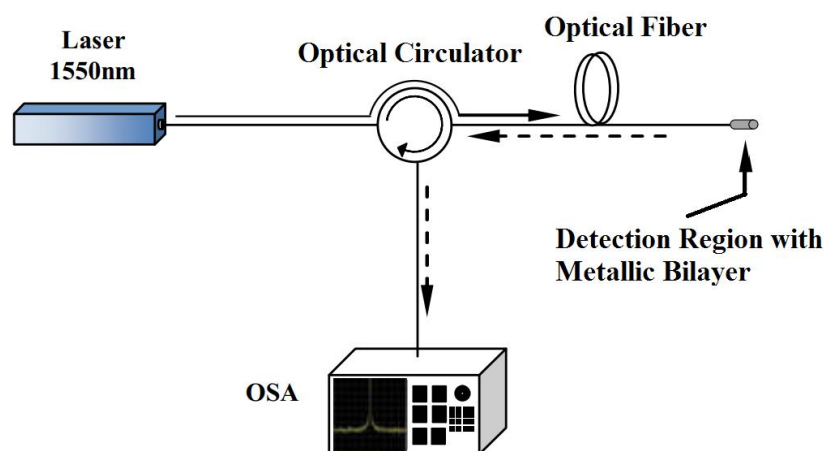

Fig. 4. Experimental setup for testing the corrosion sensor with double metallic layer.

The Ti(10 nm)/Al(10 nm) and Ni(5 nm)/Al(5 nm) bilayers were deposited on the cleaved fiber facet to form the sensor region. In Ti/Al, Ti is metal 1 (inner layer, next to the fiber) and Al is metal 2 (outer layer, next to the external medium). In Ni/Al, Ni is metal 1 and Al is metal 2. The Metal 1 / Metal 2 convention was presented in Fig. 1. The films were deposited by DC magnetron sputtering system at the end of optical fibers after cleaning and cleavage. The pressure was 2.2×10^{-7} Torr. These metals were chosen due to their great applicability in the industry, their optical reflectivity properties and the significant difference in the corrosion rate in the corrosive agents used. In addition, the position and thickness used for the metals are very important to allow the observation of the variation in the intensity of the reflected light, due to the corrosion process in the metallic films since the beginning of the corrosion. For laboratory corrosion experiments, Al-etch acid (25 H_2PO_4 : 1 HNO_3 : 5 CH_3COOH), was used, with expected corrosion rates of 50 nm/min and 2.5 nm/min, for the Al and Ni [19], [38], respectively, and Si Iso etch acid (126 HNO_3 : 60 H_2O : 5 NH_4F), with an expected corrosion rate of 60 nm/min and 300 nm/min, for the Al and Ti [19], [38], respectively. These corrosion rate values are for room temperature. The experiments in controlled laboratory conditions were performed also at room temperature.

IV. RESULTS

Fig. 5 shows the results obtained from the COMSOL numerical model considering surface roughness, the analytical model of laminar corrosion from the Fresnel equations and the experimental results for the reflectance as a function of the thickness of the thin films deposited at the end of the fiber. The values of parameter *A* of (4) are obtained by adjusting the reflectance obtained by simulations with COMSOL with the experimental one, for each value of *d*, as shown in Fig. 5 (a) and (b). For our experimental conditions, the best value found for parameter Λ is 35 nm for the result with the Ni (5nm) / Al (5nm) metal bilayer and Al-Etch as an external medium, as shown in Fig. 5 (a), and Λ = 50 nm for the Ti (10nm)/Al (10nm) bilayer and Si Iso Etch as an external medium, illustrated in Fig. 5 (b). Both results are for the wavelength of 1550 nm. It is important to highlight that the choice of thicknesses and positions of the metals in the Ni (5nm)/Al (5nm) and Ti (10nm)/Al (10nm) bilayers is related to the optical properties of the materials and was based on previous simulations, which showed that the use of these values allows rapid detection of corrosion.
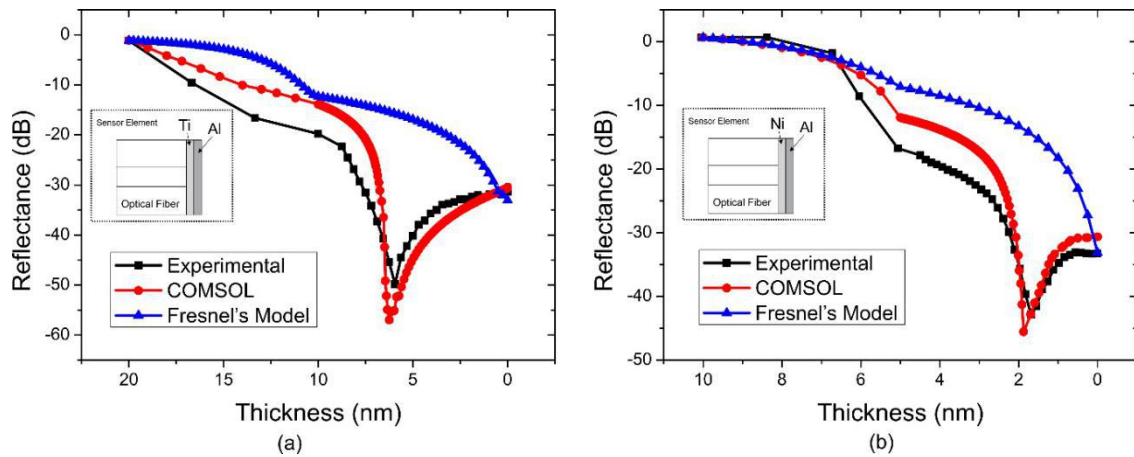
Fig. 5. Experimental, COMSOL and analytical results of the corrosion process of the bilayer (a) with Ti (10 nm)/Al (10 nm) in Si Iso Etch (b) with Ni (5 nm)/Al (5 nm) in Al-Etch.

In the reflectance curves of Fig. 5 (a), the transition point from one metal to another in the bilayer can be observed at a thickness of 10 nm, both in the experimental results and in the numerical simulations, through the change in the slope, or trend of the evolution of the reflectance curve. In addition, it is also observed that the results of the numerical model (COMSOL), which takes into account the roughness of the metallic surface caused by corrosion, are closer to the experimental results than the results of the model that considers laminar corrosion (Fresnel model), which does not consider the surface roughness. The pronounced valley in the reflectance observed for the thickness of approximately 6 nm, both in the experimental data and in the numerical simulation, is attributed to the surface plasmon resonance effect that occurs due to the presence of surface roughness, as described in [29]. Fig. 5 (b) shows the change in reflectance as a function of the thickness of the Ni (5 nm)/Al (5 nm) bilayer. Similar to the results in Fig. 5 (a), there is also a change in the trend of the reflectance curve in the transition between the metals of the bilayer, in the thickness of 5 nm. Here, the numerical model also comes closer to experimental results compared to the analytical model.

Fig. 6 shows two experimental curves obtained from two Ni (5 nm)/Al (5 nm) samples from the same fabrication batch, that is, they were fabricated at the same time as the fibers were side by side in the sputtering chamber. The fiber detection sections are immersed in the Al-Etch solution at different moments, independently. The result shows a small difference in the optical response of the sensor in the transition region between the metals, between 2.5 and 5 seconds, and in the valley region, between 44 and 50 seconds of corrosion. This difference in the corrosion process can be caused by non-uniformities in the structure of the deposited metals, or by agitation of the sample, or other variations in the conditions of the acid during corrosion. Even identical samples can generate slightly different roughness patterns due to corrosion, causing the difference in the valley of the reflectance curve. For the case of Fig. 6, the average corrosion rates with standard deviations measured for Ni and Al are (0.087 ± 0.004) nm/s and (0.916 ± 0.005) nm/s, respectively.
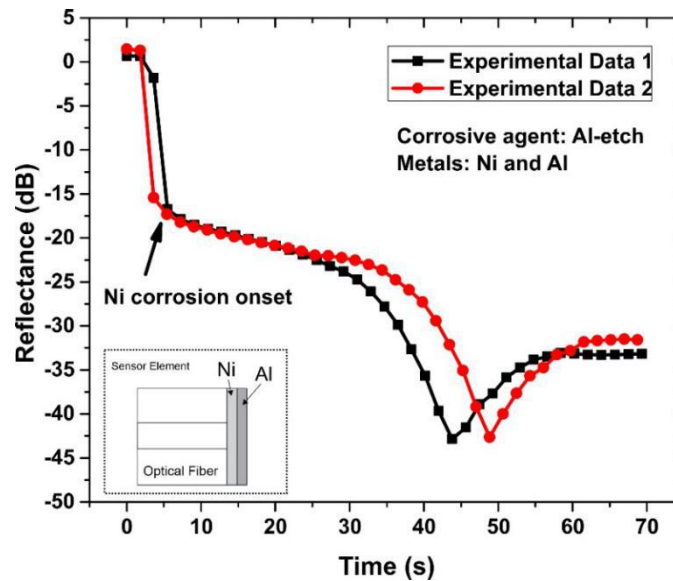
521

Fig. 6. Reflectance as a function of the corrosion time of the Ni (5 nm)/Al (5 nm) bilayer in the Al-Etch solution.

In Fig. 7, experimental results are presented in which Si Iso Etch is used in the corrosion process of a set of three sensors with Ti (10 nm)/Al (10 nm) bilayer. The results obtained from the samples show greater uniformity in the optical response of the sensor, without the variations in the valleys shown in Fig. 6, which may indicate greater uniformity in the structures of the deposited films or in the corrosion process. It is possible to observe in Fig. 7 that since the beginning of the corrosion there is a change in the reflected light. At a given point in the corrosive process, at approximately 22 seconds, the reflectance drops to a minimum and then stabilizes at a constant level. The constant level means that the corrosion process in the double metallic layer at the end of the fiber has ended. However, the minimum level of reflectance indicates that the valley is associated with the effects of light scattering and surface plasmon coupling [25], [29]. Both effects are a consequence of the formation of roughness on the surface of the metallic film caused by the corrosion process. The transition between the metals occurs around the point of thickness equal to 10 nm (3.69 seconds in Fig. 7), where it can be observed that there is a change in the slope of the reflectance curve. The observation of this change in trend gives an indication of the transition between the metals and allows the calculation of the corrosion rate of the substance in each of the metals of the bilayer. In the case of Fig. 7, the average corrosion rate measured with standard deviations for Al (outer metal layer), first to be corroded, and for Ti (inner metal layer, next to the fiber) are (2.76 ± 0.26) nm/s and (0.202 ± 0.019) nm/s, respectively.
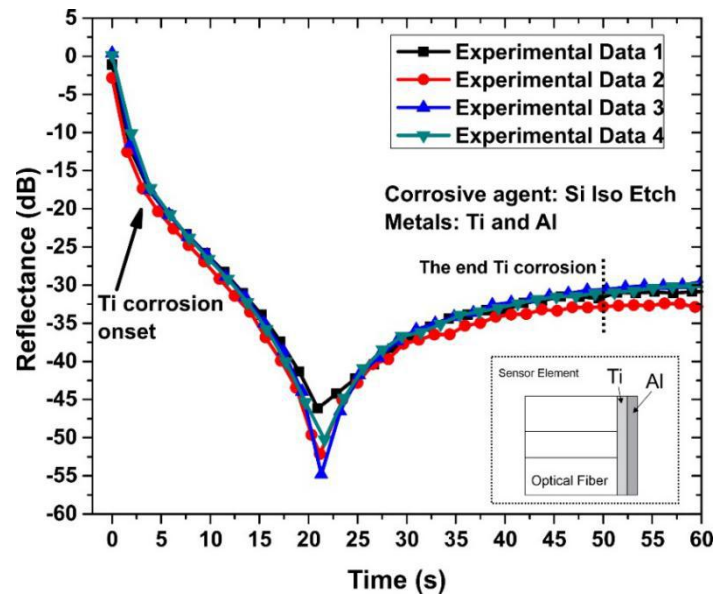
Fig. 7. Reflectance as a function of the corrosion time of the Ti (10 nm)/Al (10 nm) bilayer in the Si Iso Etch solution.

For laboratory measurements, the action of the corrosive process on the Ti (10 nm)/Al (10 nm) bilayer sensor head was also evaluated by controlled corrosion using two corrosive agents, Al-Etch and Si Iso Etch, in a sequence. The same metallic bilayer was exposed to corrosive agents at different times by manually changing the corrosive agent in a sequential action of immersing the fiber tip in acid. Fig. 8 shows the reflectance variation curves as a function of the corrosion time of the double metallic layer under this condition. The detection section is immersed in the Al-Etch solution for the corrosion of the first metal film that makes up the double layer, Al, then the detection section is immersed in the Si Iso Etch solution for the corrosion of the second metal film, the Ti. In the first 12 seconds of corrosion, the reflected power decreases approximately 9.85 dB, and the average corrosion rate for Al is 0.83 nm/s, the standard deviation obtained was null due to the transition point inserted with the change from Al-etch acid to Si Iso Etch. Then, after the immersion of the sensing region in the Si Iso Etch, the power of the reflected light decreases rapidly (40 dB in 20 seconds), reaches the valley and stabilizes on the plateau indicating that there is no more metal at the tip of the fiber. The measured average corrosion rate with standard deviation of Ti is (0.154 ± 0.001) nm/s.

As in Fig. 7, it can be seen in Fig. 8 that the data from the 3 independent experiments carried out in each case show good agreement with each other.
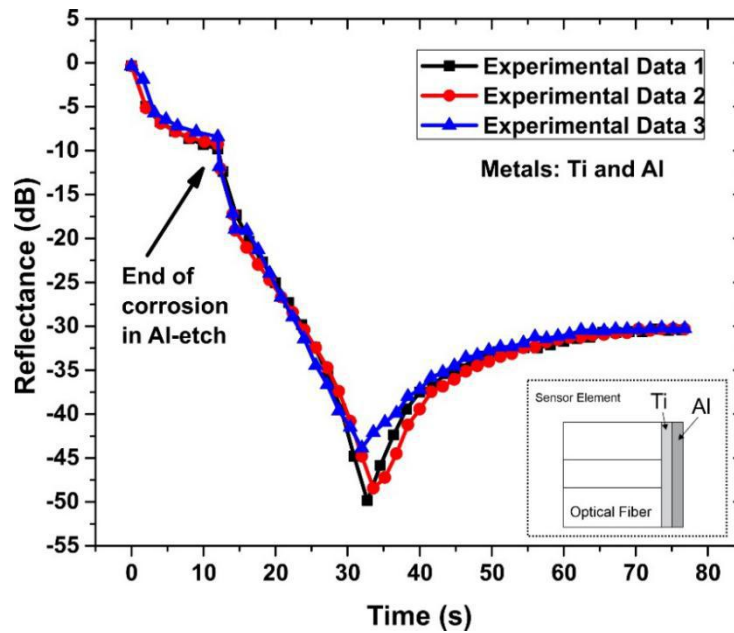
Fig. 8. Reflectance as a function of corrosion time for three samples of Ti (10 nm) / Al (10 nm) bilayers in Al-Etch and Si Iso Etch.

The values for the corrosion rates obtained from the results shown in figures 6, 7 and 8 are close to the values found in the literature [19], [38] only for Al. For Ni and mainly for Ti, the measured values are quite different from the reported values. The discrepancy between the corrosion rates obtained by the optical sensor proposed in this work and the corrosion rates obtained in [38] may be related to the measurement technique used and the material structure. This is because in [38] corrosion of metals is done in bulk and separately for each metal, while in this work corrosion is carried out on a bilayer of metallic thin films constructed by sputtering deposition. As highlighted in [39], corrosion for these two material profiles can occur at different rates. Another important aspect is the level of purity of each component of the corrosive solution, which can change the corrosion rate in a few dozen times, as described in [40].

Finally, it is important to note that the choice of metals and their thickness has an impact on the sensor's measuring interval. The proposed Ti (10 nm) / Al (10 nm) sensor presents an optimized structure with 20 nm of the metallic bilayer, with a measuring interval (20 ± 1 nm), twice that reported in [19].

V. CONCLUSIONS

In this paper, a sensor with metallic bilayer deposited on the end facet of a standard single-mode optical fiber was proposed and characterized by simulations and experimental results. Two studies were presented for the sensor region, with different thickness and metals, with Ti (10 nm)/Al (10 nm) and Ni (5 nm)/Al (5 nm) bilayers. The thickness and composition of the metallic layers were optimized via simulations.

The results showed that, depending on the optical properties and positioning of the films on the fiber, it is possible to measure the corrosion rate of each metal individually. They have also been

shown that it is possible to identify the end of corrosion of the outer metal layer, even if the corrosion rates of the metals are close, because the effect of corrosion on reflectance depends on the metal's refractive index.

The use of a bilayer, instead of a monolayer as in previous publications, improves the sensor measuring interval, mitigating the sensor blind period problem identified in monolayer structures, and provides the corrosion rate earlier during the corrosion process.

REFERENCES

[1] K. D. Bennett, L. R. McLaughlin, "Monitoring of corrosion in steel structures using optical fiber sensors," in: Smart Structures and Materials 1995: Smart Systems for Bridges, Structures, and Highways. *International Society for Optics and Photonics*, vol. 2446, pp. 48-59, 1995.

[2] J. R. Davis, "Corrosion: Understanding the Basics," *ASM International, Materials Park*, pp. 1-20, 2000.

[3] D. Luo, Y. Li, J. Li, K. S. Lim, N. A. M. Nazal, H. Ahmad, "A recent progress of steel bar corrosion diagnostic techniques in RC structures," *Sensors*, vol. 19, pp. 34, 2019.

[4] K. V. Rybalkaz, L. A. Beketaeva, A. D. Davydov, "Estimation of corrosion current by the analysis of polarization curves: Electrochemical kinetics mode," *Russian Journal of Electrochemistry*, vol. 50, pp. 108-113, 2014.

[5] E. Pinet, "Pressure measurement with fiber-optic sensors: commercial technologies and applications," 21st International Conference on Optical Fiber Sensors. *International Society for Optics and Photonics*, vol. 7753, pp. 775304, 2011.

[6] Y. Syvenkyy, B. Dewan, M. Feaver, S. B. Ip, "Commercial Phosphorescence Fiber-Optic Sensor for Long Distance Temperature Measurement," in: 26th International Conference on Optical Fiber Sensors, *OSA Technical Digest (Optical Society of America, 2018)*, pp. ThE4, 2018.

[7] L. H. Chen, T. Li, C. C. Chan R. Menon, P. Balamurali, M. Shaillender, B. Neu, X. M. Ang, P. Zu, W. C. Wong, K. C. Leong, "Chitosan based fiber-optic Fabry–Perot humidity sensor," *Sensors and Actuators B: Chemical*, vol. 169, pp. 167-172, 2012.

[8] N. Wang, W. Tian, H. Zhang, X. Yu, X. Yin, Y. Du, D. Li, "An easily fabricated high performance Fabry-Perot optical fiber humidity sensor filled with graphene quantum dots," *Sensors,* vol. 21, pp. 806, 2021.

[9] Y. Zhang, Z. Chen, W. Chen, H. Li, "Unobtrusive and continuous BCG-based human identification using a microbend fiber sensor," *IEEE Access*, vol. 7, pp. 72518-72527, 2019.

[10] D. An, X. Chen, Y. Wang, S. Gao, X. Yu, "High sensitivity microbend sensor based on anti-resonant hollow-core fiber," Asia Communications and Photonics Conference. *Optical Society of America*, pp. M4A-74, 2020.

[11] R. Magalhães, J. Pereira, O. Tarasenko, S. M. Lopez, M. G. Herráez, W. Margulis, H. F. Martins, "Towards Distributed Measurements of Electric Fields Using Optical Fibers: Proposal and Proof-Of-Concept Experiment," *Sensors*, vol. 20, pp. 4461, 2020.

[12] I. Sharma, P. R. Chaudhuri, "A new approach to sensing low electric field using optical fibers beam-deflection configuration with $BiFe_{0.9}Co_{0.1}O_3$ nanoparticles as probe and determination of polarization," *Optical Fiber Technology*, vol. 62, pp. 102472, 2021.

[13] S. Gao, C. Ji, Q. Ning, W. Chen, J. Li, "High-sensitive Mach-Zehnder interferometric temperature fiber-optic sensor based on core-offset splicing technique," *Optical Fiber Technology*, vol. 56, pp. 102202, 2020.

[14] M. S. P. Silva, H. P. Alves, J. F. Nascimento, J. F. Martins-Filho, "Impact of Pulse Width on the Sensitivity and Range of a Raman-based Distributed Fiberoptic Temperature Sensor," *Journal of Microwaves, Optoelectronics and Electromagnetic Applications*, vol. 17, pp. 539-551, 2018.

[15] N. Zhou, P. Jia, J Liu, Q. Ren, G. An, T. Liang, J. Xiong, "MEMS-based reflective intensity-modulated fiber-optic sensor for pressure measurements," Sensors, vol. 20, pp. 2233, 2020.

[16] Y. Li, S. Pu, Z. Hao, S. Yan, Y. Zhang, M. Lahoubi, "Vector magnetic field sensor based on U-bent single-mode fiber and magnetic fluid," *Optics Express*, vol. 29, pp. 5236-5246, 2021.

[17] H. J. B. de Oliveira; J. F. Martins-Filho; J. F. do Nascimento, "Computational Modeling of H_2S Gas Sensor Using Surface Plasmon Resonance in a D-Shaped Optical Fiber," in: *2018 SBFoton International Optics and Photonics Conference (SBFoton IOPC). IEEE*, pp. 1-5, 2018.

[18] S. M. M. S. Maricar, D. Sastikumar, P. R. Vanga, M. Ashok, "$BiFeO_3$ clad modified fiber optic gas sensor for room temperature applications," *Materials Today: Proceedings*, vol. 39, pp. 245-249, 2021.

[19] J. F. Martins-Filho, E. Fontana, J. Guimaraes, D. F. Pizzato, I. J. S. Coelho, "Fiber-optic-based Corrosion Sensor using OTDR," *SENSORS, 2007 IEEE*, pp. 1172-1174, 2007.

[20] N. Vahdati, X. Wang, O. Shiryayev, P. Rostron, F. F. Yap, "External corrosion detection of oil pipelines using fiber optics," *Sensors*, vol. 20, n. 3, p. 684, 2020.

[21] L. Fan, X. Tan, Q. Zhang, W. Meng, G. Chen, Y. Bao, "Monitoring corrosion of steel bars in reinforced concrete based on helix strains measured from a distributed fiber optic sensor," *Engineering Structures*, vol. 204, pp. 110039, 2020.

[22] D. Luo, J. Li, Y. Li, "A review of fiber-optic corrosion sensor in civil engineering," in: *AIP Conference Proceedings. AIP Publishing LLC*, pp. 020055, 2018.

[23] G. Qiao, Z. Zhou, J. Ou, "Thin Fe-C Alloy Solid Film Based Fiber Optic Corrosion Sensor," *2006 1st IEEE International Conference on Nano/Micro Engineered and Molecular Systems, Zhuhai*, pp. 541-544, 2006.

[24] J. F. Nascimento, M. J. Silva, I. J. S. Coêlho, E. Cipriano, J. F. Martins-Filho, "Amplified OTDR systems for multipoint corrosion monitoring," *Sensors*, vol. 12, pp. 3438-3448, 2012.

[25] E. Fontana, R. H. Pantell, "Characterization of multilayer rough surfaces by use of surface-plasmon spectroscopy," *Physical Review B*, vol. 37, pp. 3164, 1988.

[26] A. L. Barabási, H. E. Stanley, "Fractal Concepts in Surface Growth," *Cambridge University Press*, 1995.

[27] J. M. Li, L. Lü, M. O. Lai, B. Ralph, "Image-Based Fractal Description of Microstructures," *Springer Science & Business Media*, pp. 79-104, 2003.

[28] R. B. Alvarez, H. J. Martin, M. F. Horstemeyer, M. Q. Chandler, N. Williams, P. T. Wang, A. Ruiz, "Corrosion relationships as a function of time and surface roughness on a structural AE44 magnesium alloy," *Corrosion Science*, vol. 52, pp. 1635–1648, 2010.

[29] H. P. Alves, J. F. Nascimento, E. Fontana, I. J. Coêlho, J. F. Martins-Filho, "Transition Layer and Surface Roughness Effects on the Response of Metal-Based Fiber-Optic Corrosion Sensors," *Journal of Lightwave Technology*, vol. 36, pp. 2597-2605, 2018.

[30] A. B. C. Multiphysics® 5.2, "Wave Optics Module User's Guide," *Stockholm, Sweden*, 2016.

[31] A. Leung, P. M. Shankar, R. Mutharasan, "A review of fiber-optic biosensors," *Sensors and Actuators B*, vol. 125, pp. 688-703, 2007.

[32] P. B. Johnson, R. W. Christy, "Optical constants of transition metals: Ti, v, cr, mn, fe, co, ni, and pd," *Physical review B*, vol. 9, n. 12, p. 5056, 1974.

[33] M. N. Polyanskiy, "Refractive index database," *https://refractiveindex.info*. Accessed on 12-05-2020.

[34] K. M. McPeak, S. V. Jayanti, S. J. P. Kress, S. Meyer, S. Iotti, A. Rossinelli, D. J. Norris, "Plasmonic films can easily be better: Rules and recipes," *ACS Photonics*, vol. 2, pp. 326-333, 2015.

[35] A. D. Rakić, A. B. Djurišic, J. M. Elazar, and M. L. Majewski, "Optical properties of metallic films for vertical-cavity optoelectronic devices," *Applied optics*, vol. 37, pp. 5271-5283, 1998.

[36] K. J. Palm, J. B. Murray, T. C. Narayan, J. N. Munday, "Dynamic optical properties of metal hydrides," *ACS Photonics*, vol. 5, pp. 4677-4686, 2018.

[37] K. Okamoto, "Fundamentals of optical waveguides," *Academic press*, 2006.

[38] K. R. Williams, K. Gupta, M. Wasilik, "Etch rates for micromachining processing-Part II," *Journal of microelectromechanical systems*, vol. 12, pp. 761-778, 2003.

[39] K. Schlüter, C. Zamponi, A. Piorra, E. Quandt, "Comparison of the corrosion behaviour of bulk and thin film magnesium alloys," *Corrosion science*, vol. 52, pp. 3973-3977, 2010.

[40] N. Fredj, T. D. Burleigh, K. L. Heidersbach, B. R. Crowder, "Corrosion of carbon steel in waters of varying purity and velocity," In: *CORROSION 2012. OnePetro*, 2012.